Since January 2020 Elsevier has created a COVID-19 resource centre with free information in English and Mandarin on the novel coronavirus COVID-19. The COVID-19 resource centre is hosted on Elsevier Connect, the company's public news and information website.

Biomedicine & Pharmacotherapy 133 (2021) 111026

Contents lists available at ScienceDirect

Biomedicine & Pharmacotherapy

journal homepage: www.elsevier.com/locate/biopha

Alveolar epithelial glycocalyx shedding aggravates the epithelial barrier and disrupts epithelial tight junctions in acute respiratory distress syndrome

Jun Li [a,b], Zhijiang Qi [b], Dongxiao Li [c], Xiao Huang [c], Boyang Qi [c], Jiali Feng [c], Jianyu Qu [c], Xiaozhi Wang [a,c,*]

[a] School of Medicine, Cheeloo College of Medicine, Shandong University, Jinan, Shandong, 250012, China
[b] Deparetment of Pulmonary and Critical Care Medicine, Yantai Affiliated Hospital of Binzhou Medical University, YanTai, Shandong, 264100, China
[c] Department of Pulmonary and Critical Care Medicine, Binzhou Medical University Hospital, Binzhou, Shandong, 256603, China

ARTICLE INFO

Keywords:
Acute respiratory distress syndrome
Alveolar epithelial glycocalyx
Tight junction proteins
Alveolar barrier
Heparanase

ABSTRACT

The main pathophysiological mechanism of acute respiratory distress syndrome (ARDS) invovles the increase in alveolar barrier permeability that is primarily caused by epithelial glycocalyx and tight junction (TJ) protein destruction. This study was performed to explore the effects of the alveolar epithelial glycocalyx on the epithelial barrier, specifically on TJ proteins, in ARDS. We used C57BL/6 mice and human lung epithelial cell models of lipopolysaccharide (LPS)-induced ARDS. Changes in alveolar permeability were evaluated *via* pulmonary histopathology analysis and by measuring the wet/dry weight ratio of the lungs. Degradation of heparan sulfate (HS), an important component of the epithelial glycocalyx, and alterations in levels of the epithelial TJ proteins (occludin, zonula occludens 1, and claudin 4) were assessed *via* ELISA, immunofluorescence analysis, and western blotting analysis. Real-time quantitative polymerase chain reaction was used to detect the mRNA of the TJ protein. Changes in glycocalyx and TJ ultrastructures in alveolar epithelial cells were evaluated through electron microscopy. *In vivo and in vitro*, LPS increased the alveolar permeability and led to HS degradation and TJ damage. After LPS stimulation, the expression of the HS-degrading enzyme heparanase (HPA) in the alveolar epithelial cells was increased. The HPA inhibitor *N-desulfated/re-N-acetylated* heparin alleviated LPS-induced HS degradation and reduced TJ damage. *In vitro*, recombinant HPA reduced the expression of the TJ protein zonula occludens-1 (ZO-1) and inhibited its mRNA expression in the alveolar epithelial cells. Taken together, our results demonstrate that shedding of the alveolar epithelial glycocalyx aggravates the epithelial barrier and damages epithelial TJ proteins in ARDS, with the underlying mechanism involving the effect of HPA on ZO-1.

1. Introduction

Acute respiratory distress syndrome (ARDS) is the acute respiratory failure characterized by increased permeability, pulmonary edema, progressive respiratory distress, and refractory hypoxemia [1]. Although ARDS has been widely studied, its mortality remains high, ranging from 34.9%–46% [2], with only supportive therapies available. Therefore, it is critical to understand the underlying pathology of ARDS. Two pathogenetic pathways lead to ARDS: direct lung damage (pulmonary ARDS) and indirect damage (extrapulmonary ARDS) [3]. Pulmonary ARDS can be initiated on the epithelial side, whereas extrapulmonary ARDS occurs mainly on the endothelial side [4]. Alveolar epithelial cells are the primary invasion target, particularly during ARDS onset, and destruction of the epithelial barrier is a key characteristic of ARDS, with many causes, including SARS-CoV, H1N1 influenza, aspiration, and potentially SARS-CoV-2. Although extrapulmonary ARDS mainly damages endothelial cells, in large animal models of ARDS, endothelial cell damage alone cannot fully induce pulmonary edema [5]. Therefore, it is necessary to study the role of alveolar epithelial cells in ARDS pathogenesis.

The main pathophysiological change in ARDS involves destruction of the alveolar-capillary barrier, in which the alveolar barrier plays an important role [1]. At present, many studies have evaluated the pulmonary endothelial barrier. In contrast, the alveolar barrier has not been

* Corresponding author at: Department of Pulmonary and Critical Care Medicine, Binzhou Medical University Hospital, Binzhou, Shandong, 256603, China.
E-mail address: hxicuwxz@163.com (X. Wang).

https://doi.org/10.1016/j.biopha.2020.111026
Received 11 July 2020; Received in revised form 8 November 2020; Accepted 15 November 2020
Available online 24 November 2020

widely examined. In addition, the permeability of the alveolar barrier is lower than that of the vascular endothelial barrier, and thus, the alveolar barrier plays an important role in developing pulmonary edema [6]. The alveolar barrier is maintained by alveolar epithelial cells and intercellular tight junction (TJ), focal adhesions, gap junctions, and desmosomes. Among these, TJ proteins are the most critical determinants of alveolar barrier function [7–11].

The alveolar epithelial glycocalyx was discovered approximately 50 years ago and may represent an important component of the alveolar barrier [12,13]. It is a carbohydrate-rich layer lining the pulmonary epithelium, composed primarily of glycosaminoglycans (mainly heparan sulfate (HS) and chondroitin sulfate) and proteoglycans. HS is critical for pulmonary hemostasis, maintaining the parenchymal structure, and facilitating cellular signaling [14,15]. Pathological degradation of glycocalyx HS causes alveolar damage and multisystem organ failure including the development of ARDS [15]. HPA is an endo-β-D-glucuronidase, and is the only enzyme that degrades HS side chains at specific intrachain sites in mammals and selectively sheds HS from the glycocalyx [16]. Intravenous injection of heparinase III, an HS-specific bacterial glucuronidase, rapidly decreases pulmonary endothelial glycocalyx layer thickness in wild-type mice [16,17]. Notably, the non-anticoagulant *N-desulfated/re-N-acetylated* heparin (NAH) inhibits HPA in mice [18]. Our previous studies indicated that intravenous injection NAH reduced lung endothelium HS shedding and alleviated extrapulmonary ARDS development in rat models [18].

TJ is composed of transmembrane proteins such as occludins, claudins, junctional adhesion molecules, and cytoplasmic proteins such as zonula occludens (ZO)-1, ZO-2, and ZO-3 [19,20]. Occludin binds directly to ZO-1, and ZO-1 binds to the intracellular cytoskeletal proteins, suggesting that ZO acts as a bridge between TJ proteins and cytoskeletal proteins [21,22]. In addition, the interaction of claudins with ZO-1 or ZO-2 is indispensable for TJ protein formation [23]. Destruction of these proteins is closely related to ARDS [24,25]. Damage to TJ proteins not only results in the formation of alveolar exudate but also attenuates its clearance [26,27]. The prognoses of patients with ARDS with low alveolar fluid clearance rates are significantly worse than of ARDS patients with higher alveolar fluid clearance rates [28]. As the protective effect of glycocalyx can relieve ARDS development, whether intact glycocalyx protects TJs has not been well studied. We hypothesize that the shedding of glycocalyx can lead to TJ damage. To confirm this assumption, animal and cell experiments were performed in this study.

2. Materials and methods

2.1. Laboratory animals

Male C57BL/6 mice (18–23 g; 8–10 weeks old) were purchased from Jinan Pengyue Laboratory Animal Breeding Co., Ltd. (Shangdong, China) and were housed under standard conditions (22 ± 2 °C; 50 % ± 10 % relative humidity; 12-h:12-h light/dark cycle). The mice were adapted to the environment for 2–3 days before the experiments. All animal experiments and feeding methods complied with the guidelines for the Care and Use of Laboratory Animals established by the US National Institutes of Health and were approved by the Binzhou Medical University Institutional Review Board.

2.2. Animal model of ARDS

Animals were randomly divided into six groups: control, lipopolysaccharide (LPS), heparinase III, LPS + NAH, heat-inactivated (HI) heparinase-III, and NAH groups. To induce LPS-mediated lung injury, the animals were intratracheally administered 5 mg/kg LPS (from *Escherichia coli* O55:B5, L2880, Sigma-Aldrich St. Louis, MO, USA) or saline (50 μL) and sacrificed 6 h later. The heparinase III group and the HI heparinase-III group were intratracheally administered 0.5 U heparinase III or 0.5 U HI heparinase-III (from *Flavobacterium heparinum*, Sigma-Aldrich, H8891), respectively, and sacrificed 1 h later [17]. We inactivated heparinase-III by heating it at 100 °C for 5 min. The LPS + NAH group and NAH group were pretreated with 150 μg NAH (Sigma-Aldrich, A8036, administered *via* 200 μL subcutaneous injection) [18,29], and one hour later, mice in the LPS and LPS + NAH groups were treated with 100 μg/mL LPS for 6 h. The bronchoalveolar lavage fluid (BALF), serum samples, and lung tissue samples were harvested.

2.3. Histopathological examination of the lungs

Mouse lung tissues were collected and fixed with 4% paraformaldehyde for 48 h. The tissues were processed, embedded in paraffin, and sectioned into 4-μm-thick slices. After hematoxylin and eosin staining, the slides were observed under an optical microscope. Lung injury was characterized by alveolar congestion and hemorrhage, alveolar neutrophil infiltration and aggregation, and thickening of the alveolar walls. Samples were scored based on the presence or absence of each feature (0, minimal; 1, mild; 2, moderate; 3, severe; and 4, maximal). For each sample, six high-magnification fields were randomly scored for each feature, and the scores were combined to generate average lung injury scores [30].

2.4. Lung wet/dry (W/D) ratios

The lung tissues were harvested and weighed with filter paper; this weight was recorded as the wet weight (W). The tissues were dehydrated at 60 °C for 48 h and weighed to obtain the dry weight (D). The W/D ratio was used to evaluate the degree of pulmonary edema.

2.5. Contents of HS in the BALF and BALF/serum of mice

After the mice were harvested, the alveoli were repeatedly lavaged with 500 μL PBS three times to obtain the BALF. The BALF of each sample was centrifuged at 900 ×g for 10 min at 4 °C, and the supernatant was collected. The blood samples were collected from the eyeballs of the mice and centrifuged at 1500 ×g for 20 min. The levels of HS in the BALF and serum were evaluated with corresponding ELISA kits (Shanghai Enzyme-linked Biotechnology Co., Shanghai, China; ml111013) in accordance with the manufacturer's instructions.

2.6. Cell culture

Human pulmonary epithelial cells (A549 cells) were purchased from the Institute of Biochemistry and Cell Biology, Chinese Academy of Science (Shanghai, China). The cells were cultured in Dulbecco's modified Eagle's medium supplemented with 10 % fetal bovine serum in a humidified incubator with 5% CO_2 at 37 °C. The cells were also separated into six groups: control, LPS, heparinase III, LPS + NAH, HI heparinase-III, and NAH group. The heparinase III and NAH concentrations used were based on the results of preliminary experiments and previous reports [18,31]. The control group was cultured in complete culture medium without LPS treatment, and cells in the LPS + NAH group and NAH group were pretreated with 10 μg/mL NAH for 1 h, after which the cells were thoroughly washed with PBS twice and replaced with complete medium. At 1 h, cells in the LPS and LPS + NAH groups were treated with 100 μg/mL LPS for 6 h. Cells in the heparinase III and HI heparinase-III groups were treated with 0.1 U/mL heparinase III or HI heparinase-III respectively for 1 h. In the recombinant HPA experiment, alveolar epithelial cells were divided into a control group and recombinant HPA group. Cells in the recombinant HPA group were treated with recombinant HPA (2 μg/mL, APA711Hu01, Cloud-clone Corp., Wuhan, China) for 12 h.

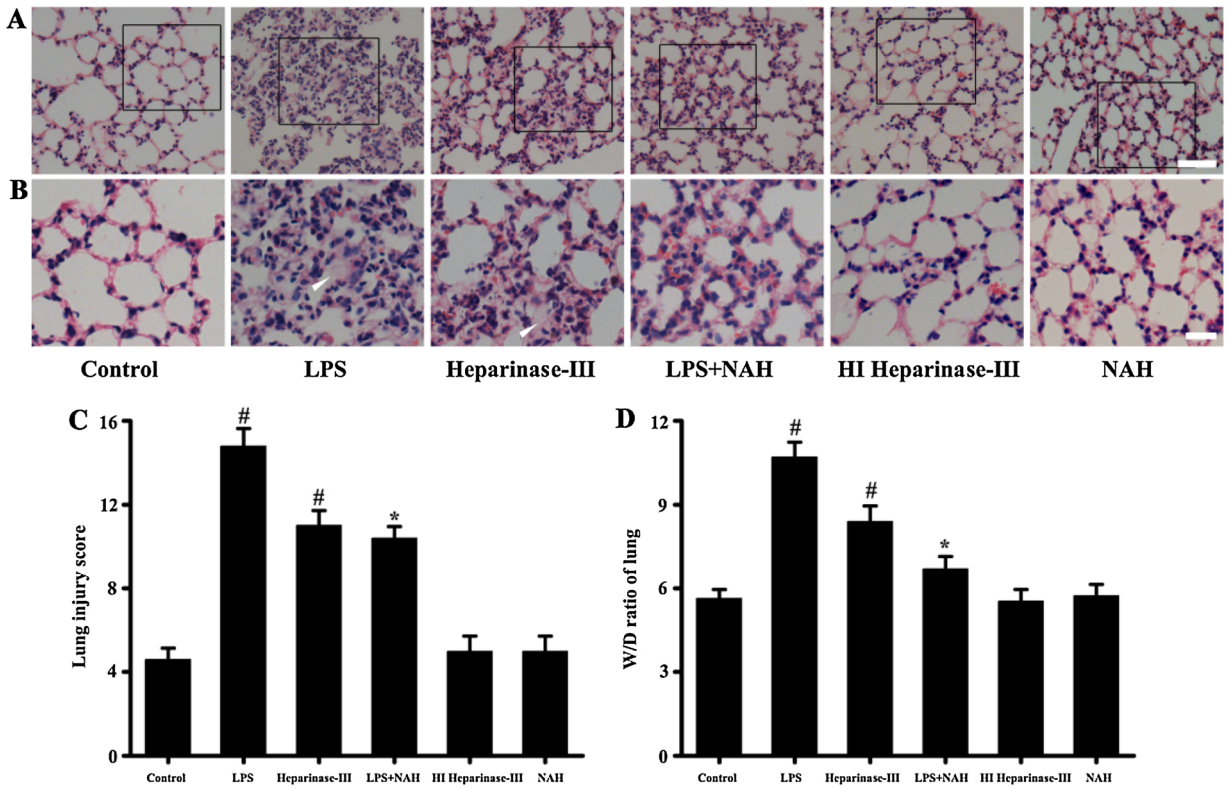

Fig. 1. Changes in the lung histopathology and W/D ratios of ARDS mice. The lung tissues of mice in the control, LPS, heparinase III, LPS + NAH, heat-inactivated heparinase-III, and NAH groups were observed *via* hematoxylin and eosin staining (A-C), and the lung W/D ratios (D; n = 6 mice/group)were measured. A Magnification, × 200; scale bar, 50 μm. B Magnification, × 400; scale bar, 20 μm. Data represent the mean ± SD of three independent experiments. $^{\#}P < 0.05$ compared to the control group; $^{*}P < 0.05$ compared to the LPS group.

2.7. Content of HPA and deciduous HS in cell supernatant

The supernatant of each group was collected, and heparanase concentration in the supernatant was measured with an human HPA Enzyme Assay kit (cat. no. E01H0100; BlueGene, Shanghai, China) according to the manufacturer's protocol. HS levels in the supernatant were evaluated with the corresponding ELISA kits (Shanghai Enzyme-linked Biotechnology Co., Ltd. ml061639) in accordance with the manufacturer's instructions.

2.8. Immunofluorescence

Lung tissues were sectioned into 4-μm-thick slices, deparaffinized with xylene, and then dehydrated with an ethanol gradient. After thermal repair of the antigens, the samples were blocked with goat serum for 30 min at room temperature and than incubated overnight at 4 °C with primary antibodies against HS (1:200; Biotechnology, Massagno, Switzerland), occludin (1:200; Invitrogen, Carlsbad, CA, USA; 33–1500), surfactant protein C (SP-C, a marker of alveolar epithelial cells [32]); (1:800; Abcam, Cambridge, UK, ab40879), ZO-1 (1:200; Invitrogen, 61–7300), or claudin 4 (1:200; Abcam, ab15104). The slides were incubated with fluorescein isothiocyanate -conjugated secondary antibodies for 1 h at room temperature. The sections were incubated with 4′,6-diamidino-2-phenylindole (Sigma-Aldrich, D8417) for 8 min, and the slices were sealed with fluorescence decay-resistant medium. The samples were imaged with a fluorescence microscope (Olympus, Tokyo, Japan), and the Image-J software (National Institutes of Health, Bethesda, MD, USA) was used to quantitatively assess the fluorescence intensities.

Human cells were fixed with 4% paraformaldehyde for 15 min and then blocked with goat serum for 1 h. The cells were incubated with antibodies against HS, occludin, or ZO-1 overnight at 4℃ and then with fluorescein isothiocyanate-conjugated anti-rabbit IgG or rhodamine-conjugated anti-mouse IgG (Beijing Zhongshan Golden Bridge Biotechnology, Beijing, China) for 1 h. The cells were imaged, and fluorescence intensities were quantified as described earlier.

2.9. Western blotting analysis

After treatment, A549 cells were lysed on ice in radioimmunoprecipitation buffer supplemented with phenylmethylsulfonyl fluoride. The lysates were centrifuged at 13,800 × *g* for 20 min at 4 °C, and protein concentrations in the supernatant were determined using a BCA Protein Assay kit (Beyotime Biotechnology, Beijing, China). Protein samples were boiled in Laemmli buffer, resolved through sodium dodecyl sulfate-polyacrylamide gel electrophoresis, and transferred to polyvinylidene difluoride membranes. The membranes were washed three times for 5 min with Tris-buffered saline containing Tween 20 and sealed with 5% skim milk at room temperature for 2 h. Then the membranes were incubated with primary antibodies against occludin (1:1000), claudin 4 (1:1000), ZO-1 (1:500), and β-Actin (1:1000; Bioss, Shanghai, China, bs-0061R) overnight at 4℃. Thereafter, the membranes were washed with Tris-buffered saline containing Tween 20 and then incubated with horseradish peroxidase-conjugated goat anti-rabbit and goat anti-mouse IgGs (Beijing Biosynthesis Biotechnology Co., Ltd., Beijing, China) for 1 h at room temperature. Bands were visualized using an electrochemiluminescence kit (Millipore, Billerica, MA, USA). Densitometry analysis was performed in the Image-J software.

2.10. Electron microscopy

To visualize epithelial glycocalyx and TJ protein structures between pulmonary epithelial cells *via* electron microscopy, the mice were anesthetized and perfused with a solution composed of 2%

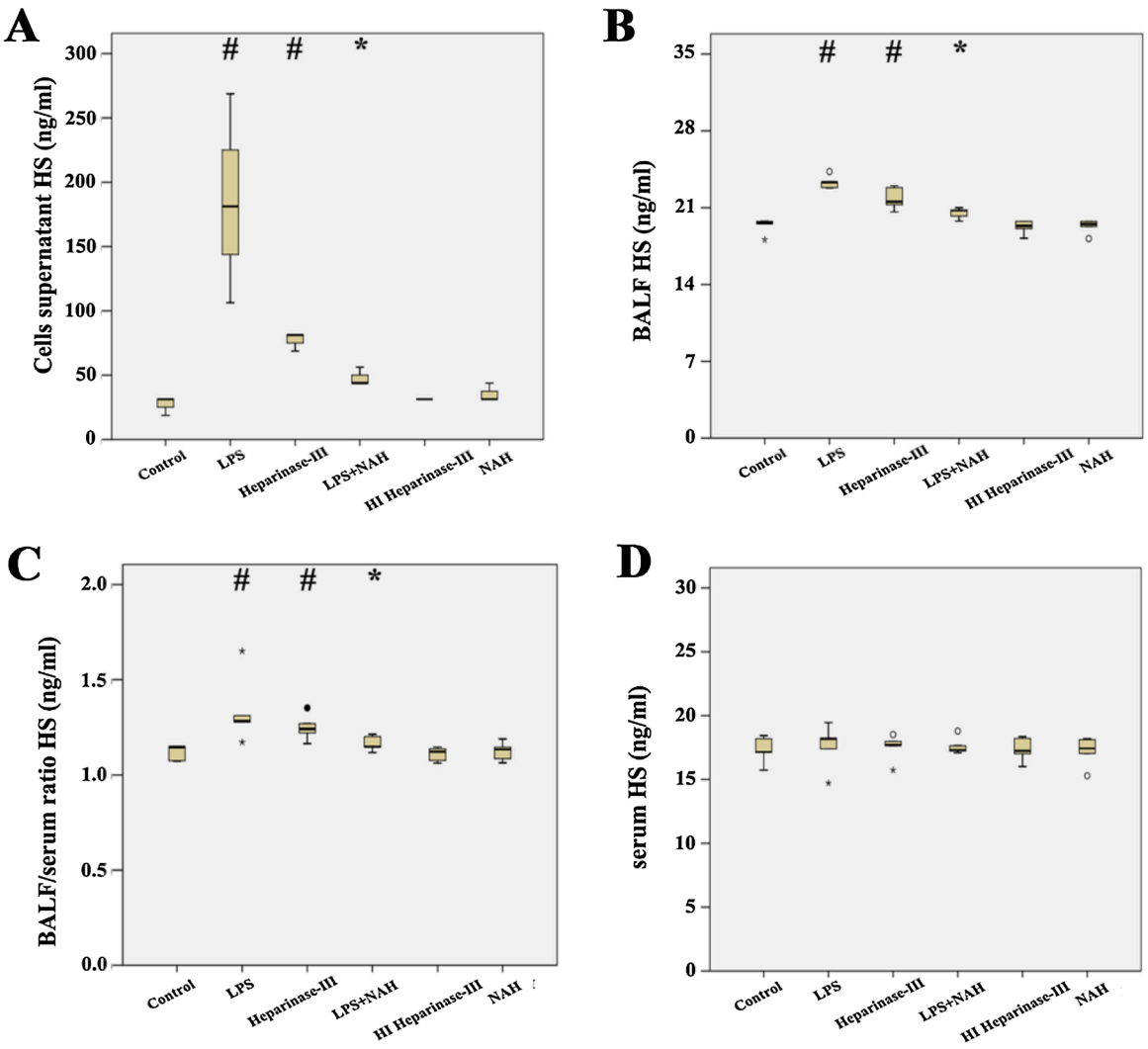

Fig. 2. Detection of HS in the supernatant of human alveolar epithelial cells and in mouse BALF and BALF/serum. HS epithelial glycocalyx degradation products in the cell supernatant of the cell were evaluated using ELISA (A). HS levels in the BALF, BALF/serum ratio, and blood of mice were detected with ELISA kits (B-D). Compared with the control group, HS degradation increased in the LPS group and heparinase III group and decreased in the LPS + NAH group. $^{\#}P < 0.05$ compared to the control group; $^{*}P < 0.05$ compared to the LPS group.

glutaraldehyde, 0.1 M sodium cacodylate buffer (pH 7.3), 2% sucrose, and 2% anthanum nitrate through a cannula placed in the left ventricle. The lung tissue was fixed and cut into 1- mm^3-sized slices. The slices were it were immersed in fixation solution for 2 h, soaked overnight in solution without glutaraldehyde, and washed with alkaline (0.03 mol/L NaOH) saccharose (2%) solution. After contrast enhancement with a solution containing 2% osmium tetroxide and 2% lanthanum nitrate, embedding in araldite, and microtomic sectioning, electron microscopy was performed.

2.11. Quantitative real-time PCR

For quantitative PCR analyses, total RNA was extracted from A549 cells using RNAiso Plus(Takara, Shiga, Japan). RNA was reverse-transcribed into cDNA with the RevertAid First Strand cDNA Synthesis Kit (Takara). Quantitative real-time PCR was performed with 50 ng of cDNA and TB Green® Fast qPCR Mix (Takara) using an Thermal Cycler Dice Real Time System (Bio-Rad Laboratories, Hercules, CA, USA). Relative expression of the target genes was normalized to *Gapdh* levels, and the ΔΔCt method was used to calculate relative expression levels. The primer sequences are listed as follows. ZO-1(forward:5′-ATAAAGTGCTGGCTTGGTCTG TTTG-3:reverse:5′-GCACTGCCCACCCATCTGTA-3). GAPDH(forward:5′-GCACCGTCAAGGCTGAGAAC-3; reverse:5′-TGGTGAAGACGCCAGTGGA-3).

2.12. Statistical analysis

Statistical analysis was conducted with SPSS 22.0 software (*SPSS Inc., Chicago, IL, USA*). For normally distributed data, continuous variables were presented as mean ± standard deviation. One-way analysis of variance and least significant difference test were applied for multi-group comparisons. For data with skewed distributions, variables were expressed as median (25th and 75th percentiles). The Kruskal-Wallis test was applied for multi-group comparisons, and Mann-Whitney *U* test was performed for two-group. $P < 0.05$ was considered statistically significant.

3. Results

3.1. Changes in lung pathology and alveolar permeability

Inflammatory cell infiltration and alveolar exudation were increased and the alveolar septum was thickened in the LPS and heparinase III

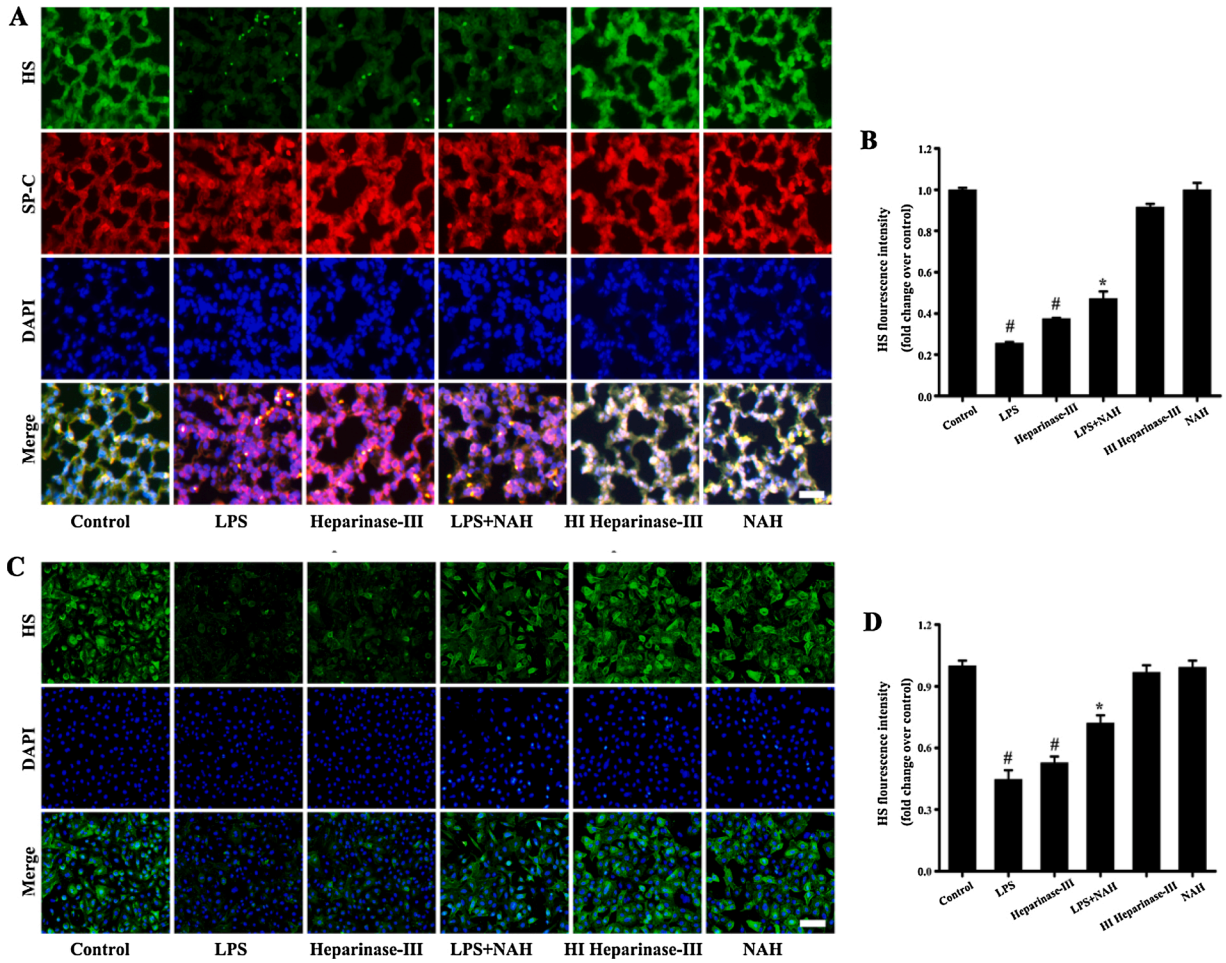

Fig. 3. Changes in alveolar epithelial HS levels *in vivo and in vitro*. (A, B) HS distributions in the alveolar epithelium of mice in the control, LPS, heparinase III, LPS + NAH, HI heparinase-III, and NAH groups (A) and associated fluorescence intensity analysis (B). In A, HS is shown in green, whereas the alveolar epithelial cell marker SP-C is shown in red. Scale bars: 50 μm. (C, D) HS distributions in A549 cells in the control, LPS, heparinase III, LPS + NAH, HI heparinase-III, and NAH groups (C) and associated fluorescence intensity analysis (D). In C, HS is shown in green. Scale bars: 100 μm. Data represent the mean ± SD of three independent experiments. $^{\#}P < 0.05$ compared to the control group; $^{*}P < 0.05$ compared to the LPS group. (For interpretation of the references to colour in this figure legend, the reader is referred to the web version of this article.

groups compared to the control group. These pathological changes were alleviated by NAH pretreatment (Fig. 1A-C). The W/D ratios of lung tissues from the LPS and heparinase III groups were significantly higher than in the control group, indicating increased pulmonary edema, whereas the ratios for mice pretreated with NAH were significantly lower than those of the LPS group ($P < 0.05$) (Fig. 1D).

3.2. Changes in HS in mouse BALF and BALF/serum and content of HS in cell supernatant

The HS content in BALF of mice confirmed that epithelial HS degradation increased after LPS stimulation and after heparinase III treatment compared to the control group. After using NAH, the epithelial HS content in BALF was lower than that in the LPS group ($P < 0.05$) (Fig. 2B). Moreover, the ratio of HS in the BALF/serum (Fig. 2C) and content of HS in the cell supernatant (Fig. 2A) showed a consistent trend. However, there was no significant difference in the blood HS levels in each group (Fig. 2D).

3.3. Changes in alveolar epithelial HS levels in vivo and in vitro

HS expression was significantly decreased in lung tissues from the LPS and heparinase III groups compared to the control group. Compared with the LPS group, the LPS + NAH group displayed attenuated reductions expression in HS ($P < 0.05$) (Fig. 3A, B). Consistently, in A549 cells, HS expression was decreased in the LPS and heparinase III groups compared to the control group. This decrease in HS expression was inhibited by pretreatment with NAH ($P < 0.05$) (Fig. 3C, D).

3.4. Changes of TJ proteins in vivo and in vitro

Immunofluorescence analysis revealed that in mice, occludin (Fig. 4A, B), claudin 4 (Fig. 4C, D) and ZO-1 (Fig. 4E, F) expression was significantly decreased after glycocalyx destruction in the LPS and heparinase III groups. NAH pretreatment resulted in increased expression of these proteins compared to the LPS group. Occludin (Fig. 5A) and ZO-1 (Fig. 5B) expression was significantly decreased in human alveolar epithelial cells after the loss of HS in the LPS and heparinase III groups, whereas the LPS + NAH group displayed increased expression of these proteins compared to the LPS group.

Furthermore, we detect occludin (Fig. 5C, D), claudin 4 (Fig. 5E, F) and ZO-1 (Fig. 5G, H) expression was confirmed in human alveolar epithelial cells through western blotting analysis. TJ proteins were significantly decreased after the loss of HS in the LPS and heparinase III groups, whereas the LPS + NAH group displayed increased expression of these proteins compared to the LPS group ($P < 0.05$).

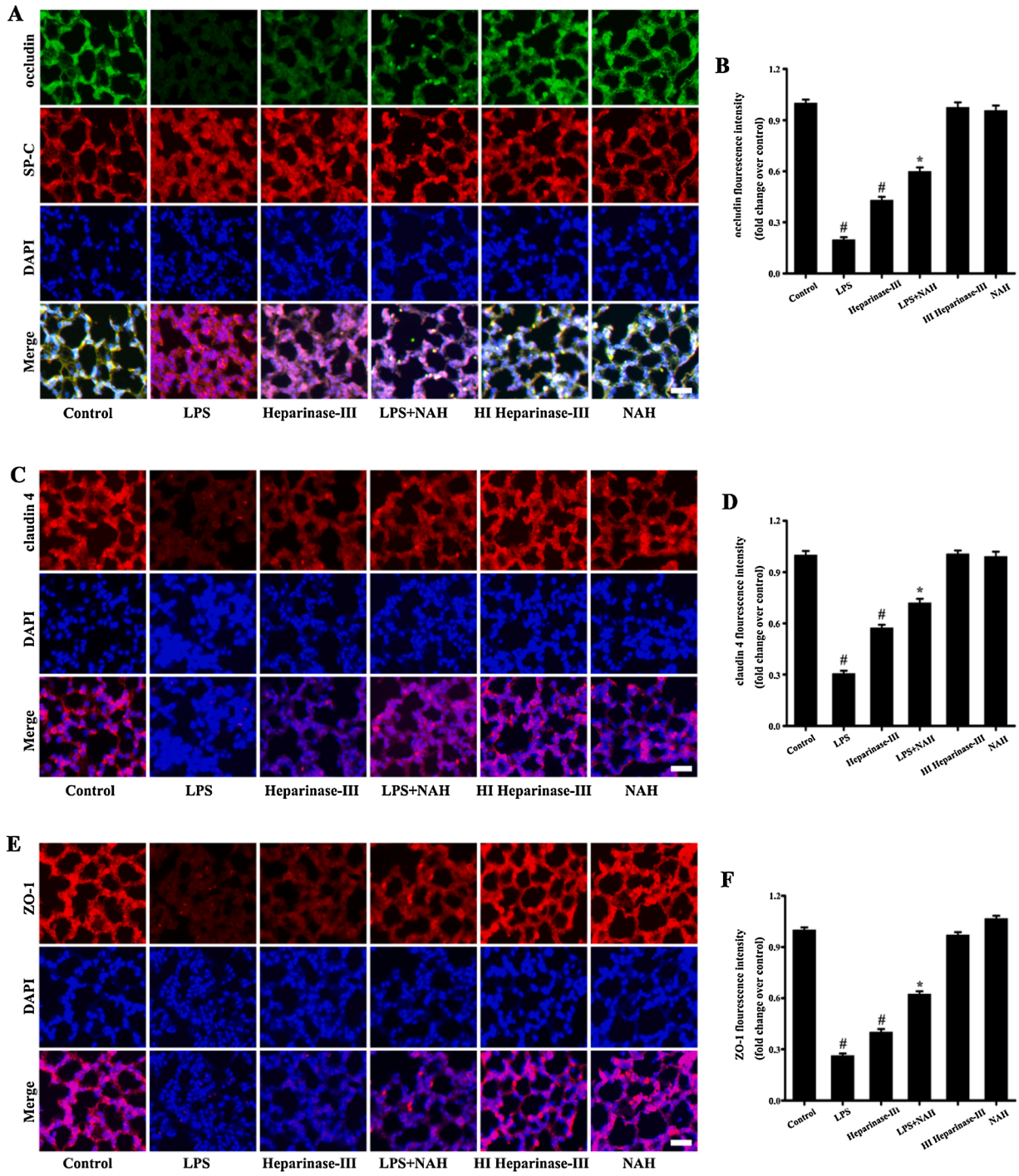

Fig. 4. Changes in alveolar epithelial TJ proteins in mice. Distributions of TJ proteins occludin (A, green), claudin 4 (C, red), and ZO-1 (E, red) and associated fluorescence intensity analysis of occludin (B), claudin 4 (D), and ZO-1 (F) in the lungs of mice in the control, LPS, heparinase III, LPS + NAH, HI heparinase-III, and NAH groups. Alveolar epithelial cells were detected using SP-C (red). Scale bar: 50 μm. Data represent the mean ± SD of three independent experiments. $^{\#}P < 0.05$ compared to the control group; $^{*}P < 0.05$ compared to the LPS group. (For interpretation of the references to colour in this figure legend, the reader is referred to the web version of this article).

3.5. Ultrastructural changes in the alveolar epithelial glycocalyx and TJ integrity in lungs of mice

The control group mice displayed a continuous, dense glycocalyx covering the alveolar epithelial cells. The glycocalyx of mice in the LPS group was completely or partially lost. Additionally, the glycocalyx was moderately affected in the NAH pretreatment group (Fig. 6A).

The control group mice showed normal and intact TJ protein structures, whereas the LPS group showed loss of TJ structures, as evidenced by an intermittently widened distance between cells, indicating the loss in TJ protein integrity. However, these changes were improved in the NAH pretreatment group (Fig. 6B).

3.6. Changes in HPA level in the supernatant of alveolar epithelial cells

HPA expression in the supernatants of alveolar epithelial cells in the control group and LPS group was detected by ELISA. Compared with the control group, HPA expression in the LPS group was significantly

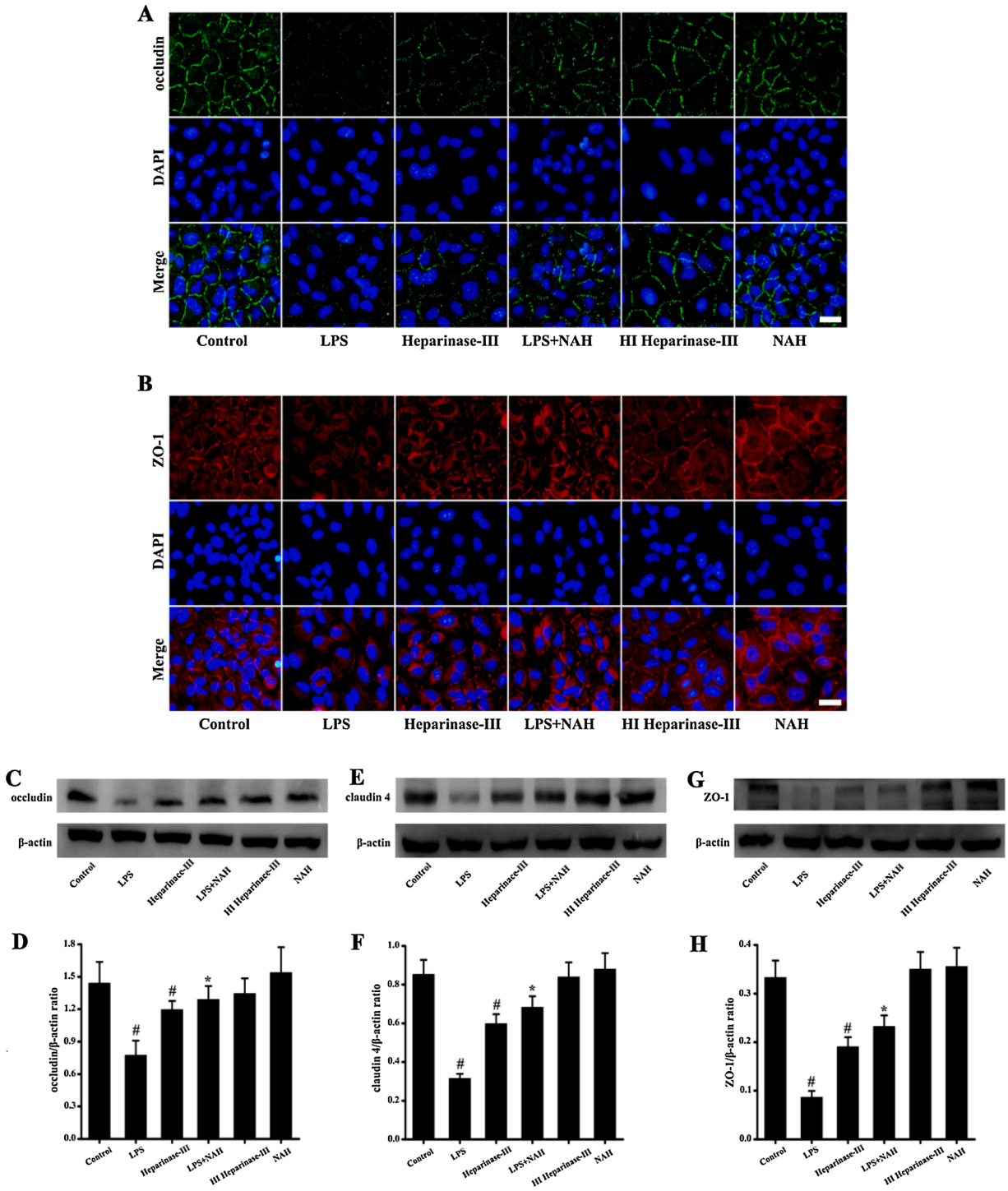

Fig. 5. Changes in TJ proteins in A549 cells. Immunofluorescence images of occludin (A, green) and ZO-1 (B, red) in A549 cells in the control, LPS, heparinase III, LPS + NAH, HI heparinase-III, and NAH groups. Scale bar: 20 μm. (C, E, and G) Western blotting analysis to determine occludin, claudin 4, and ZO-1 levels in A549 cells from each group. Quantifications of occludin, claudin 4, and ZO-1 are shown in (D), (F), and (H) respectively. β-Actin was used as a loading control. Data represent the mean ± SD of three independent experiments. $^{\#}P < 0.05$ compared to the control group; $^{*}P < 0.05$ compared to the LPS group. (For interpretation of the references to colour in this figure legend, the reader is referred to the web version of this article).

increased ($P < 0.05$) (Fig. 7).

3.7. Effects of recombinant HPA on HS in human alveolar epithelial cells

Through immunofluorescence analysis, we demonstrated that HS level in alveolar epithelial cells of the recombinant HPA group was significantly reduced compared to the control group ($P < 0.05$) (Fig. 8A, C).

3.8. Effects of recombinant HPA on TJ protein expression in human alveolar epithelial cells

Immunofluorescence analysis showed that in the control group, the staining intensity of ZO-1 was strongly positive in human alveolar

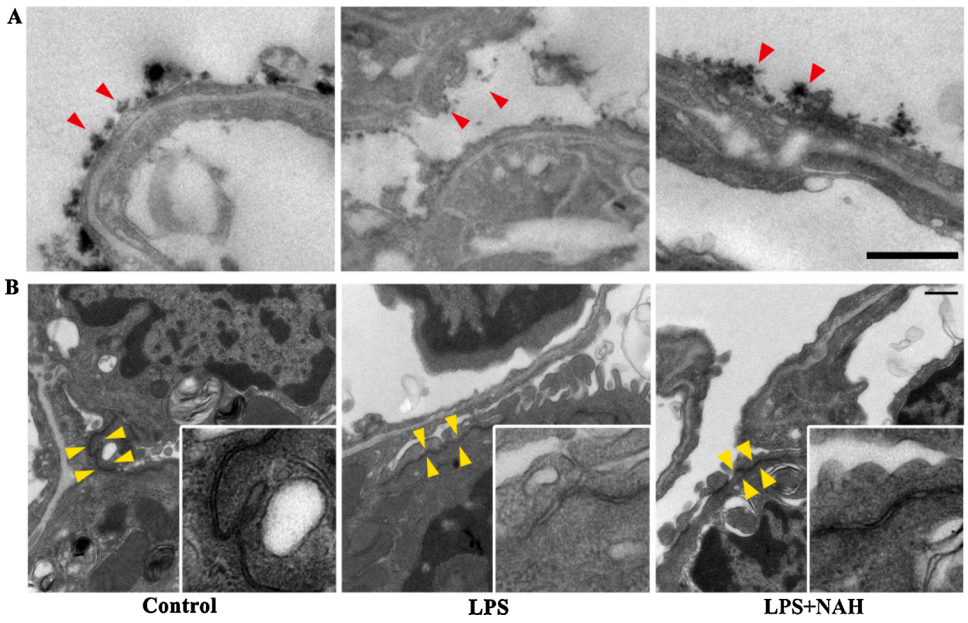

Fig. 6. Ultrastructural changes in alveolar epithelial cell glycocalyx and the TJ protein integrity in the lungs of mice. Lung tissues were collected to analyze pulmonary epithelial glycocalyx (A, red arrow, scale bar: 0.5 μm) and TJ protein (B, yellow arrow, scale bar: 0.5 μm) ultrastructures *via* TEM imaging. (For interpretation of the references to colour in this figure legend, the reader is referred to the web version of this article).

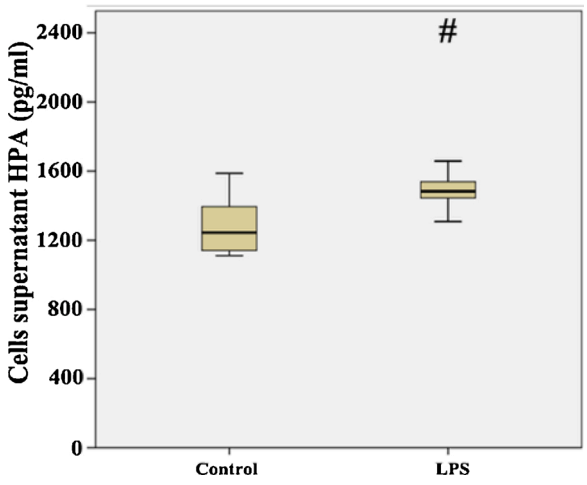

Fig. 7. Changes in HPA levels in supernatant of alveolar epithelial cells. HPA was determined in alveolar epithelial cells in the control and LPS groups *via* ELISA. $^{\#}P < 0.05$ compared to the control group.

epithelial cells, with a continuous and undulating distribution along the cell membrane (Fig. 8B). However, in the recombinant HPA group, ZO-1 lost its normal continuous distribution in epithelial cells.

Furthermore, we validated the expression of ZO-1 in human alveolar epithelial cells *via* western blotting (Fig. 8D, E). The recombinant HPA group inhibited the protein expression of ZO-1, resulting in a particularly dramatic decrease in ZO-1 expression ($P < 0.05$).

The mRNA levels of *ZO-1* in human alveolar epithelial cells were remarkably decreased after recombinant HPA challenge compared to the control group (***$P < 0.001$) (Fig. 8F).

4. Discussion

In this study, an animal ARDS model induced by intratracheal instillation of LPS [33]and A549 cell injury model were used to observe the LPS-induced glycocalyx and TJ changes in ARDS epithelial cells. The results showed that LPS can lead to increased degradation of the epithelium glycocalyx component HS and destruction of TJ proteins (ZO-1, occludin, claudin 4), increasing the permeability of the alveolar barrier and exudation of inflammatory cells.

A549 cells are human alveolar epithelial cells that are commonly used in *in vitro* alveolar epithelial cell research [34,35]. We further observed the shedding of the cleavage product HS of the glycocalyx and increased the expression of HS in the cell supernatant after LPS stimulation. Through *in vivo* experiments, we found that HS expression in the BALF of the model group was significantly increased; however, the BALF/serum ratio was increased, but blood HS was not significantly increased, confirming that HS shedding after LPS stimulation occurred mainly because of the glycocalyx of the alveolar epithelium.

The barrier of the alveolar epithelium is composed of the alveolar epithelium, alveolar epithelial glycocalyx, and TJs of epithelial cells. HS is the main component of glycocalyx, which plays an important role in the epithelial barrier [36]. Studies have shown that increased HS damage can lead to increased alveolar permeability and ARDS formation [36,37], affecting the recovery of lung injury [38]; these results are similar to those reported above in this study.

HPA is the only enzyme selectively shedding HS. In this study, the increase in the HPA content in the supernatant of cells indicates that HS destruction is related to the increase in HPA content stimulated by LPS. To confirm the role of HPA in LPS-induced lung injury, we added exogenous heparinase III to obtain HS degradation results similar to that of LPS. Further addition of the HPA competitive antagonist NAH [17] can reverse this phenomenon. Therefore, LPS can increase HPA, which in turn leads to HS degradation. The integrity of the glycocalyx of alveolar epithelial cells is destroyed, leading to increased alveolar barrier permeability followed by lung injury or ARDS.

TJ protein is an important determinant of the epithelial barrier [7–11]. Occludin, ZO-1, and claudin 4 are important components of the alveolar epithelial TJ protein. In this study, both the LPS-treated animal and cell models revealed that with the HS destruction, the TJ protein was also showed destroyed. The ELISA results showed that HPA expression in the cell supernatant of the LPS group was significantly increased; after exogenous addition of heparinase III, the TJ was also destroyed. NAH pretreatment prevents the effect of HPA, can reverse destruction of the glycocalyx, and reduces the destruction of TJs,

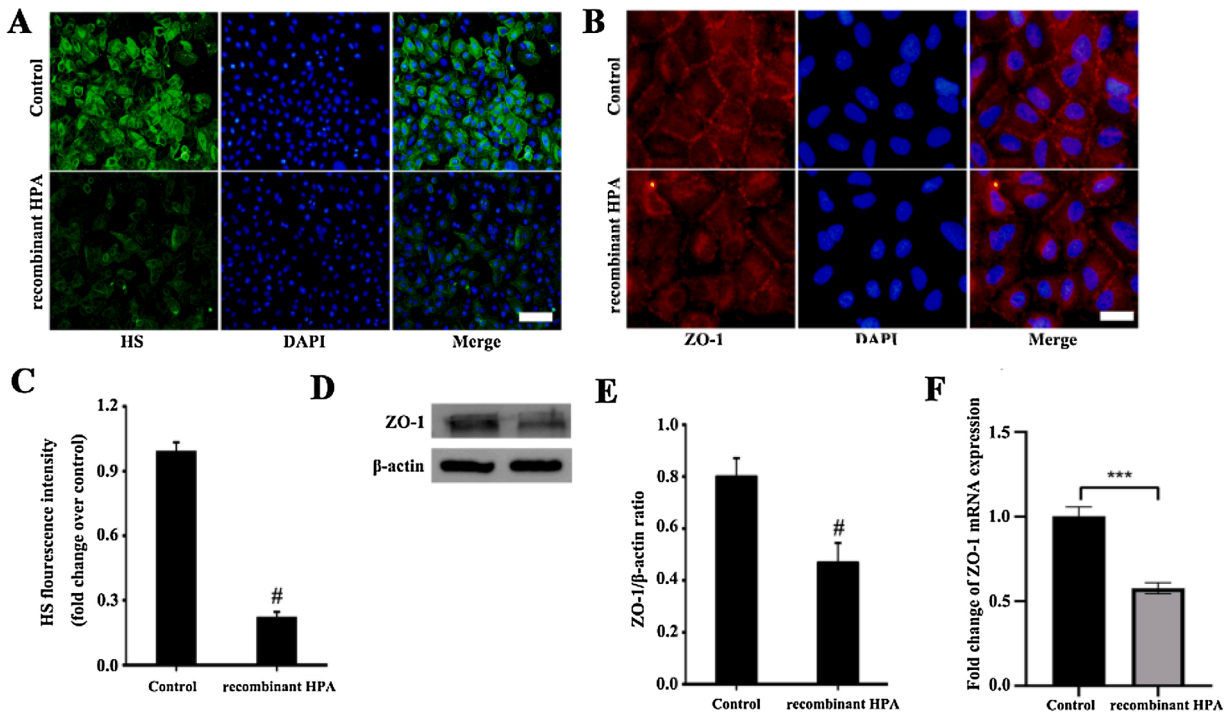

Fig. 8. Effects of recombinant HPA on HS and TJ proteins in human alveolar epithelial cells. Immunofluorescence images of HS (A, green) and associated fluorescence intensity analysis of HS(C) in A549 cells in the control and recombinant HPA groups. Scale bar: 100 μm. $^{\#}P < 0.05$ compared to the control group. Immunofluorescence images of ZO-1 (B, red) in human alveolar epithelial cells in the control and recombinant HPA groups. Scale bar: 20 μm. Western blotting analysis of ZO-1 (D) levels in A549 cells in the control and recombinant HPA groups. Quantifications of ZO-1 are shown in (E). β-Actin was used as a loading control. Data represent the mean ± SD of three independent experiments. $^{\#}P < 0.05$ compared to the control group. mRNA levels of *ZO-1* in the human alveolar epithelial cells evaluated *via* qRT-PCR (F). $^{***}P < 0.001$ compared to the control group. (For interpretation of the references to colour in this figure legend, the reader is referred to the web version of this article).

suggesting that the protection of glycocalyx HS also protects TJs. Based on this, there may be a certain relationship between HPA-HS-TJ.

It is unclear whether there is an inherent relationship between the shedding of glycocalyx HS and the damage of TJ. To further study the relationship between TJs and HPA, we used recombinant HPA (endogenous HPA) to treat the cells. The results showed that recombinant HPA significantly decreased the expression of ZO-1 protein and *ZO-1* mRNA. ZO-1 plays an important role in the development of ARDS [21,25]. ZO-1 is the cytoskeleton protein of the cell junction protein, and its destruction can affect the binding of occludin and claudin 4 to ZO-1, resulting in formation of cell cracks [21,22]. When ZO-1 was depleted in epithelial cells, barrier-forming proteins such as claudin and occludin could not assemble into the strands normally found in TJ proteins, and the epithelial barrier effect of TJ proteins was completely eliminated [23, 39]. To explore the mechanism of HPA-HS on ZO-1, we assessed the *ZO-1* mRNA. Our study indicated that HPA-HS may interfere with ZO-1 synthesis and then affect TJ proteins assembling and function.

Syndecan 1 (SDC-1), another component of glycocalyx, acts in synergy with TJ through Stat3 signaling [40]. To explore whether HPA-HS uses the same signaling pathway as SDC-1 does for affecting TJs, we studied the HPA-HS-Stat3 pathway by performing *in vitro* experiments. The western blotting results showed that the decrease in the phosphorylation level of Stat3 in cells stimulated by recombinant HPA did not significantly differ from that of the normal group (data not shown). Therefore, the signaling pathway *via* which HPA affects ZO-1 differs from that of SDC-1. To identify the pathway through by which HPA-HS affects ZO-1 expression, further studies are needed.

This study has some limitations. First, we only studied changes in epithelial TJ proteins after alveolar epithelial glycocalyx HS shedding. Further analyses are required to determine whether other components of the glycocalyx, such as SDC-1, SDC-4, and chondroitin sulfate, are related to epithelial TJ proteins. Second, many proteins are involved in TJs; however, few have been studied. Therefore, whether glycocalyx also affects should be further analyzed.

5. Conclusion

Our results demonstrate that shedding of the alveolar epithelial glycocalyx affected the expression of TJ proteins (occludin, ZO-1, and claudin 4) and disrupted TJ, and this effect was reversed by NAH. The mechanism by which glycocalyx affects TJ proteins partly involves HPA, which suppresses the expression of ZO-1. Protecting glycocalyx may reduce TJ damage and improve the alveolar barrier, reduce pulmonary edema, and provide new therapeutic targets for ARDS treatment.

Declaration of Competing Interest

None.

Acknowledgements

This work was supported by funding from the National Natural Science Foundation of China (no. 81670078) and Taishan Scholar Project of Shandong Province.

References

[1] B.T. Thompson, R.C. Chambers, K.D. Liu, Acute respiratory distress syndrome, N. Engl. J. Med. 377 (6) (2017) 562–572, https://doi.org/10.1056/NEJMra1608077.

[2] G. Bellani, J.G. Laffey, T. Pham, E. Fan, L. Brochard, A. Esteban, L. Gattinoni, F. van Haren, A. Larsson, D.F. McAuley, M. Ranieri, G. Rubenfeld, B.T. Thompson, H. Wrigge, A.S. Slutsky, A. Pesenti, L.S. Investigators, E.T. Group, Epidemiology, patterns of care, and mortality for patients with acute respiratory distress syndrome in intensive care units in 50 countries, JAMA 315 (8) (2016) 788–800, https://doi.org/10.1001/jama.2016.0291.

[3] K. Anan, K. Kawamura, M. Suga, K. Ichikado, Clinical differences between pulmonary and extrapulmonary acute respiratory distress syndrome: a retrospective cohort study of prospectively collected data in Japan, J. Thorac. Dis. 10 (10) (2018) 5796–5803, https://doi.org/10.21037/jtd.2018.09.73.

[4] P. Pelosi, D. D'Onofrio, D. Chiumello, S. Paolo, G. Chiara, V.L. Capelozzi, C. S. Barbas, M. Chiaranda, L. Gattinoni, Pulmonary and extrapulmonary acute respiratory distress syndrome are different, Eur. Respir. J. Suppl. 42 (2003) 48s–56s, https://doi.org/10.1183/09031936.03.00420803.

[5] J.P. Wiener-Kronish, K.H. Albertine, M.A. Matthay, Differential responses of the endothelial and epithelial barriers of the lung in sheep to *Escherichia coli* endotoxin, J. Clin. Invest. 88 (3) (1991) 864–875, https://doi.org/10.1172/JCI115388.

[6] K. Brune, J. Frank, A. Schwingshackl, J. Finigan, V.K. Sidhaye, Pulmonary epithelial barrier function: some new players and mechanisms, Am. J. Physiol. Lung Cell Mol. Physiol. 308 (8) (2015) L731–L745, https://doi.org/10.1152/ajplung.00309.2014.

[7] C.E. Overgaard, L.A. Mitchell, M. Koval, Roles for claudins in alveolar epithelial barrier function, Ann. N. Y. Acad. Sci. 1257 (2012) 167–174, https://doi.org/10.1111/j.1749-6632.2012.06545.x.

[8] S. Boitano, Z. Safdar, D.G. Welsh, J. Bhattacharya, M. Koval, Cell-cell interactions in regulating lung function, Am. J. Physiol. Lung Cell Mol. Physiol. 287 (3) (2004) L455–L459, https://doi.org/10.1152/ajplung.00172.2004.

[9] M. Koval, Sharing signals: connecting lung epithelial cells with gap junction channels, Am. J. Physiol. Lung Cell Mol. Physiol. 283 (5) (2002) L875–L893, https://doi.org/10.1152/ajplung.00078.2002.

[10] M. Koval, Claudin heterogeneity and control of lung tight junctions, Annu. Rev. Physiol. 75 (2013) 551–567, https://doi.org/10.1146/annurev-physiol-030212-183809.

[11] K.P. Wesslau, A. Stein, M. Kasper, K. Barth, P2X7 receptor indirectly regulates the JAM-A protein content via modulation of GSK-3beta, Int. J. Mol. Sci. 20 (9) (2019), https://doi.org/10.3390/ijms20092298.

[12] A.Z. Chignalia, F. Yetimakman, S.C. Christiaans, S. Unal, B. Bayrakci, B. M. Wagener, R.T. Russell, J.D. Kerby, J.F. Pittet, R.O. Dull, The glycocalyx and trauma: a review, Shock 45 (4) (2016) 338–348, https://doi.org/10.1097/SHK.0000000000000513.

[13] S.M. Haeger, X. Liu, X. Han, J.B. McNeil, K. Oshima, S.A. McMurtry, Y. Yang, Y. Ouyang, F. Zhang, E. Nozik-Grayck, R.L. Zemans, R.M. Tuder, J.A. Bastarache, R.J. Linhardt, E.P. Schmidt, Epithelial heparan sulfate contributes to alveolar barrier function and is shed during lung injury, Am. J. Respir. Cell Mol. Biol. 59 (3) (2018) 363–374, https://doi.org/10.1165/rcmb.2017-0428OC.

[14] S.M. Haeger, Y. Yang, E.P. Schmidt, Heparan sulfate in the developing, healthy, and injured lung, Am. J. Respir. Cell Mol. Biol. 55 (1) (2016) 5–11, https://doi.org/10.1165/rcmb.2016-0043TR.

[15] W.B. LaRiviere, E.P. Schmidt, The pulmonary endothelial glycocalyx in ARDS: a critical role for heparan sulfate, Curr. Top. Membr. 82 (2018) 33–52, https://doi.org/10.1016/bs.ctm.2018.08.005.

[16] D. Chappell, M. Jacob, M. Rehm, M. Stoeckelhuber, U. Welsch, P. Conzen, B. F. Becker, Heparinase selectively sheds heparan sulphate from the endothelial glycocalyx, Biol. Chem. 389 (1) (2008) 79–82, https://doi.org/10.1515/BC.2008.005.

[17] E.P. Schmidt, Y. Yang, W.J. Janssen, A. Gandjeva, M.J. Perez, L. Barthel, R. L. Zemans, J.C. Bowman, D.E. Koyanagi, Z.X. Yunt, L.P. Smith, S.S. Cheng, K. H. Overdier, K.R. Thompson, M.W. Geraci, I.S. Douglas, D.B. Pearse, R.M. Tuder, The pulmonary endothelial glycocalyx regulates neutrophil adhesion and lung injury during experimental sepsis, Nat. Med. 18 (8) (2012) 1217–1223, https://doi.org/10.1038/nm.2843.

[18] X. Huang, S. Han, X. Liu, T. Wang, H. Xu, B. Xia, G. Kong, J. Li, W. Zhu, H. Hu, D. Hao, X. Wang, Both UFH and NAH alleviate shedding of endothelial glycocalyx and coagulopathy in LPS-induced sepsis, Exp. Ther. Med. 19 (2) (2020) 913–922, https://doi.org/10.3892/etm.2019.8285.

[19] C. Wray, Y. Mao, J. Pan, A. Chandrasena, F. Piasta, J.A. Frank, Claudin-4 augments alveolar epithelial barrier function and is induced in acute lung injury, Am. J. Physiol. Lung Cell Mol. Physiol. 297 (2) (2009) L219–L227, https://doi.org/10.1152/ajplung.00043.2009.

[20] A. Hartsock, W.J. Nelson, Adherens and tight junctions: structure, function and connections to the actin cytoskeleton, Biochim. Biophys. Acta 1778 (3) (2008) 660–669, https://doi.org/10.1016/j.bbamem.2007.07.012.

[21] O.H. Wittekindt, Tight junctions in pulmonary epithelia during lung inflammation, Pflugers Arch. 469 (1) (2017) 135–147, https://doi.org/10.1007/s00424-016-1917-3.

[22] Laurel S. Rodgers, et al., Epithelial barrier assembly requires coordinated activity of multiple domains of the tight junction protein ZO-1, J. Cell. Sci. 126 (Pt 7) (2013) 1565–1575, https://doi.org/10.1242/jcs.113399.

[23] K. Umeda, J. Ikenouchi, S. Katahira-Tayama, K. Furuse, H. Sasaki, M. Nakayama, T. Matsui, S. Tsukita, M. Furuse, S. Tsukita, ZO-1 and ZO-2 independently determine where claudins are polymerized in tight-junction strand formation, Cell. 126 (4) (2006) 741–754, https://doi.org/10.1016/j.cell.2006.06.043.

[24] B. Schlingmann, C.E. Overgaard, S.A. Molina, K.S. Lynn, L.A. Mitchell, S. Dorsainvil White, A.L. Mattheyses, D.M. Guidot, C.T. Capaldo, M. Koval, Regulation of claudin/zonula occludens-1 complexes by hetero-claudin interactions, Nat. Commun. 7 (2016) 12276, https://doi.org/10.1038/ncomms12276.

[25] X. Lin, M. Barravecchia, P. Kothari, J.L. Young, D.A. Dean, beta1-Na(+),K(+)-ATPase gene therapy upregulates tight junctions to rescue lipopolysaccharide-induced acute lung injury, Gene Ther. 23 (6) (2016) 489–499, https://doi.org/10.1038/gt.2016.19.

[26] D. Rokkam, M.J. Lafemina, J.W. Lee, M.A. Matthay, J.A. Frank, Claudin-4 levels are associated with intact alveolar fluid clearance in human lungs, Am. J. Pathol. 179 (3) (2011) 1081–1087, https://doi.org/10.1016/j.ajpath.2011.05.017.

[27] W. Jin, L. Rong, Y. Liu, Y. Song, Y. Li, J. Pan, Increased claudin-3, -4 and -18 levels in bronchoalveolar lavage fluid reflect severity of acute lung injury, Respirology 18 (4) (2013) 643–651, https://doi.org/10.1111/resp.12034.

[28] L.B. Ware, M.A. Matthay, Alveolar fluid clearance is impaired in the majority of patients with acute lung injury and the acute respiratory distress syndrome, Am. J. Respir. Crit. Care Med. 163 (6) (2001) 1376–1383, https://doi.org/10.1164/ajrccm.163.6.2004035.

[29] M.I. Lygizos, Y. Yang, C.J. Altmann, K. Okamura, A.A. Hernando, M.J. Perez, L. P. Smith, D.E. Koyanagi, A. Gandjeva, R. Bhargava, R.M. Tuder, S. Faubel, E. P. Schmidt, Heparanase mediates renal dysfunction during early sepsis in mice, Physiol. Rep. 1 (6) (2013) e00153, https://doi.org/10.1002/phy2.153.

[30] F. Aeffner, B. Bolon, I.C. Davis, Mouse models of acute respiratory distress syndrome, Toxicol. Pathol. 43 (8) (2015) 1074–1092, https://doi.org/10.1177/0192623315598399.

[31] M. Nikmanesh, Z.D. Shi, J.M. Tarbell, Heparan sulfate proteoglycan mediates shear stress-induced endothelial gene expression in mouse embryonic stem cell-derived endothelial cells, Biotechnol. Bioeng. 109 (2) (2012) 583–594, https://doi.org/10.1002/bit.23302.

[32] M.F. Beers, Y. Moodley, When is an alveolar type 2 cell an alveolar type 2 cell? A conundrum for lung stem cell biology and regenerative medicine, Am. J. Respir. Cell Mol. Biol. 57 (1) (2017) 18–27, https://doi.org/10.1165/rcmb.2016-0426PS.

[33] Y. Zhou, Y. Yang, T. Liang, Y. Hu, H. Tang, D. Song, H. Fang, The regulatory effect of microRNA-21a-3p on the promotion of telocyte angiogenesis mediated by PI3K (p110alpha)/AKT/mTOR in LPS induced mice ARDS, J. Transl. Med. 17 (1) (2019) 427, https://doi.org/10.1186/s12967-019-02168-z.

[34] W.-C. Lin, C.-W. Chen, Y.-W. Huang, L. Chao, J. Chao, Y.-S. Lin, C.-F. Lin, Kallistatin protects against sepsis-related acute lung injury via inhibiting inflammation and apoptosis, Sci. Rep. 5 (1) (2015), https://doi.org/10.1038/srep12463.

[35] I. Vadasz, R.E. Morty, M.G. Kohstall, A. Olschewski, F. Grimminger, W. Seeger, H. A. Ghofrani, Oleic acid inhibits alveolar fluid reabsorption: a role in acute respiratory distress syndrome? Am. J. Respir. Crit. Care Med. 171 (5) (2005) 469–479, https://doi.org/10.1164/rccm.200407-954OC.

[36] V.J. Coulson-Thomas, S.H. Chang, L.K. Yeh, Y.M. Coulson-Thomas, Y. Yamaguchi, J. Esko, C.Y. Liu, W. Kao, Loss of corneal epithelial heparan sulfate leads to corneal degeneration and impaired wound healing, Invest. Ophthalmol. Vis. Sci. 56 (5) (2015) 3004–3014, https://doi.org/10.1167/iovs.14-15341.

[37] S. Chen, Y. He, Z. Hu, S. Lu, X. Yin, X. Ma, C. Lv, G. Jin, Heparanase mediates intestinal inflammation and injury in a mouse model of Sepsis, J. Histochem. Cytochem. 65 (4) (2017) 241–249, https://doi.org/10.1369/0022155417692536.

[38] W.B. LaRivière, et al., Alveolar heparan sulfate shedding impedes recovery from bleomycin-induced lung injury, American journal of physiology, Am. J. Physiol. Lung Cell Mol. Physiol. 318 (6) (2020) L1198–L1210, https://doi.org/10.1152/ajplung.00063.2020.

[39] P. Pulimeno, S. Paschoud, S. Citi, A role for ZO-1 and PLEKHA7 in recruiting paracingulin to tight and adherens junctions of epithelial cells, J. Biol. Chem. 286 (19) (2011) 16743–16750, https://doi.org/10.1074/jbc.M111.230862.

[40] Z. Wang, R. Li, J. Tan, L. Peng, P. Wang, J. Liu, H. Xiong, B. Jiang, Y. Chen, Syndecan-1 acts in synergy with tight junction through Stat3 signaling to maintain intestinal mucosal barrier and prevent bacterial translocation, Inflamm. Bowel Dis. 21 (8) (2015) 1894–1907, https://doi.org/10.1097/MIB.0000000000000421.